Grid-connected Virtual Synchronous Machine using Virtual Inertia Control

Om Prakash Jaiswal [1]*, Sandeep Dhami [1], Jhala Nath Kafle [2,3]

[1]Department of Electrical Engineering, Pashchimanchal Campus, Institute of Engineering, Tribhuvan University, Pokhara, Nepal

[2]Department of Electrical Engineering, Pulchowk Campus, Institute of Engineering, Tribhuvan University,

[3]Lalitpur Metropolitan City, Lalitpur District, Bagmati Province, Nepal

*omp98660@gmail.com

(Manuscript Received: 31st December, 2025; Revised: 11th May, 2026; Accepted: 12th May, 2026)

Abstract

System frequency stability becomes more difficult to maintain as system inertia steadily declines due to quick spread of inverter based renewable energy. Virtual Synchronous Generator (VSG) control is one of major solutions to this problem since it makes grid-connected inverters mimic inertial and damping properties of traditional synchronous machines. This paper is about modeling, control design and dynamic performance study of VSG inverter using virtual impedance-based architecture in MATLAB/Simulink. The control structure involves incorporating virtual inertia and damping through active power-frequency droop, reactive power-voltage regulation as well as inner voltage-current control loops. Virtual inertia constant (J) and damping coefficient (D) are varied one after the other during step power reference changes. It has been seen that a bigger value of J causes the transient swings to be more intense and the time to come back to normal level to be longer. Whereas with a low D the active power can overshoot up to 34% and the reactive power troughs can be almost three times deeper than those with high damping ones. Eventually all the responses reach the same steady states implying that J and D are purely dynamic parameters. Fast, well damped responses with minimum overshoot are the result of moderate inertia and intermediate damping that corresponds to optimal performance. Such results reveal the very basic inertia-damping trade-off in VSG designs and show that coordinated adjusting of the parameters is a must for a stable transient and a reliable incorporation of renewable energy.

Keywords: Non-linear averaged model (NLAM), Virtual impedance, Virtual Synchronous Generator (VSG), Virtual Synchronous Machine (VSM)

1. Introduction

Because of the increasing worldwide energy shortage and the fast progress of clean energy sources technology, the production of clean energy has become a main area of research (Jakhar et al., 2016; Liu et al., 2019; Worthmann et al., 2015). However, unlike big central power plants that mostly depend on the operation of synchronous generators (SG), distributed generation (DG) units have hardly any or no physical rotating or spinning mass, inertia, or damping characteristics (Bevrani et al., 2014). As the share of inverter-based resources (IBRs) increases, Mostly in weak or developing power systems, issues like poor frequency control, less damping, and higher chances of system instability may occur (Moore et al., 2025).

The idea of a virtual synchronous machine (VSM), sometimes called a virtual synchronous generator (VSG), is a very promising approach to controlling inverters that are connected to the grid. This will allow grid-connected inverters to overcome the issues mentioned (Neupane & Poudel, 2024). Inverters controlled by VSM can not only stabilize the grid's frequency and voltage but also enhance the transient response and provide synthetic or virtual inertia during disturbances since they operate in a manner similar to synchronous generators by using virtual inertia and damping.

Many researchers focus on studying and emphasizing the vital role of VSM in facilitating frequency stability and inertia in a low-inertia, renewable energy-based power system. A literature review presents the principle and effectiveness of VSGs and other forms of virtual inertia and grid-forming methods that provide frequency support in scenarios of large renewable integration to the system (Li et al., 2025). New control methods of VSG have been introduced to ensure a seamless transition in the changes from grid-connected to islanded modes with improved voltage and phase regulation (Citro et al., 2024). Adaptive VSG controllers with frequency integral correction Really enhance the inertia and damping features and Because of this, result in improved dynamic response to large load disturbances (Rajak & Pudur, 2025).

Virtual synchronous generators (VSGs) are being used in microgrids, hybrid renewable systems, and low-inertia power networks (D'Arco & Suul, 2013). VSGs act like synchronous generators by giving virtual inertia and damping, stabilizing voltage and frequency, and making it simpler for the inverter-based renewable energy sources to be integrated. The initial VSG control system was based on voltage and current regulation to make PWM signals. This led to the current ones with virtual speed and excitation regulators (Neupane, 2025; Neupane & Poudel, 2024). In their papers, the authors (Neupane & Poudel, 2024) and (Neupane, 2025) highlight a simple version of the controller discussed in the journal (D'Arco et al., 2015), which regulates voltage and current to produce a PWM signal for a VSM. Stability of system and sensitivity to parameters experiments demonstrate that the VSG controller is robust and flexible under different operations (Yao et al., 2015).

The rapid expansion of photovoltaic (PV) systems is becoming a challenge for the stability of the power grid. That's because the PV systems connected through inverters hardly have the natural inertia and damping features that synchronous generators have. This lack of aspects has led to difficulties in frequency and voltage regulation (Tahir et al., 2024). In the initial PV-VSG systems, use was made of DC-link capacitors to give inertial support. Still, this limited the implementation of Maximum Power Point Tracking (MPPT), which in turn, diminished the energy usage (Yan et al., 2018; Zarina et al., 2014). Still, this problem has been resolved with the aid of advanced control techniques like master-slave, event-triggered, and coordinated BESS-VSG strategies that enable efficient power sharing and optimal PV output while maintaining grid support (He et al., 2023; Liang et al., 2023; Qu & Wang, 2021; Sangwongwanich et al., 2017).

Detailed small-signal models of PV-VSG systems which comprise DC-DC converters, virtual impedance, and VSG control loops have been used to study stability, fine-tune controller parameters, and improve low-frequency oscillation damping (Deng et al., 2020). Taking into account the DC-side dynamics and self-adaptive rotor inertia, the improved PV-VSG controllers working under variable PV conditions have demonstrated better stability and power production (Ding et al., 2019).

Grid-forming inverters with droop control or virtual synchronous generator (VSG) features contribute to better fault handling and power sharing in microgrid contexts. Still, short-lived mismatches can occur due to integration with synchronous machines. Transient virtual impedance and similar methods that restrict current but do not cause voltage reduction or controller overdrive enable stability and fast inverter response at the same time (Paquette & Divan, 2015; Rocabert et al., 2012).

Ultimately, the progress reveals that VSGs, Mainly, when paired with energy storage systems, can Quite a bit enhance the stability, dynamic flexibility, and integration of renewables of modern power systems based on inverters. They address the issues of low inertia and highly variable grids.

In this work, the grid-connected VSG model suggested by (Neupane & Poudel, 2024) was used and reproduced in MATLAB/Simulink as a benchmark system for further investigation. The original work mainly concerns the implementation and operation of the VSG model and to produce datasets for data-driven modeling. The effect of the virtual inertia (J) and Damping constant (D) on the dynamic behavior of the system were not deeply studied. Hence, this research studies the effect of changing

inertia and damping parameters on active power (P), reactive power (Q) and VSG angular velocity (ω_{vsm}) under grid-connected operating conditions.

The rest of the paper is organized as follows: The research mythology including NLAM and control loop strategy used is presented in Section 2, the MATLAB/Simulink model is described in Section 3. Validation and findings are covered in Section 4. The discussion of the study is discussed in Section 5 and concluded in Section 6. Section 7 presents the future recommendations for the study.

2. Research Methodology

2.1 Non-linear average model (NLAM)

In modern power system, high-frequency switching is used by converter-based resources (CBRs) to converter AC to DC and DC to AC. An averaged method known as the Non-Linear Averaged Model (NLAM) is used to capture the system's non-linear dynamics without requiring an excessive amount of computer work because simulating every switching event is computationally costly. The primary objective of NLAM is to simplify the computationally complex detailed switching model while preserving the system's non-linear dynamic behavior over an extended period of time.

Fig. 1 adapted from (Neupane, 2025), represents the model that includes both the control and power stages for a voltage source converter (VSC) in a VSM architecture. The power control loops, virtual impedance, current and voltage regulators, and other components of the control system simulate the damping and inertial characteristics of a synchronous generator.

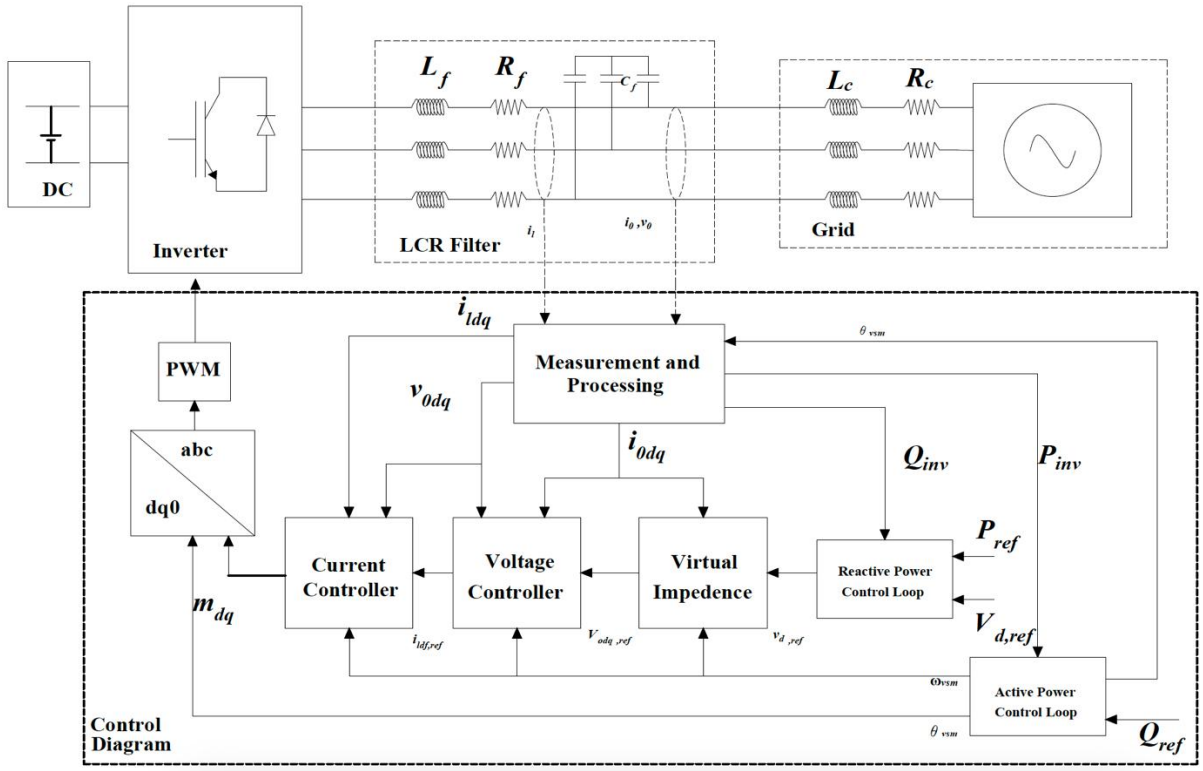

Fig. 1: Overall block diagram of grid-connected virtual synchronous machine.

Differential equations are used to describe slower dynamics in the physical layer of the system, which includes the power electronic inverter, its semiconductor switching devices, the interfacing filters and the grid interface. Averaging is use to approximate high-frequency switching. This method makes it possible to analyze stability, dynamic response, and controller design through precise and efficient simulations.

2.1.1 Inverter, filter, coupling impedance average model

The dynamic interface between the converter and the grid in grid-connected inverter systems is defined by the filter, coupling impedance, and inverter average model. The system of equations for the filter current, voltage, and coupling impedance in $dq0$ frame is represented in Equation 1 where, R_f, L_f and C_f denotes the filter resistance, inductance, and capacitance respectively. R_c, L_c denotes the grid coupling resistance and inductance respectively. Similarly, (i_{ld}, i_{lq}), (v_{od}, v_{oq}) and (i_{od}, i_{oq}) are the dq components of the filter current, filter voltage and grid current, respectively.

$$\left.\begin{aligned}
\frac{di_{ld}}{dt} &= -\frac{R_f}{L_f} i_{ld} + \omega_{vsm} i_{lq} + \frac{v_{id} - v_{cd}}{L_f} \\
\frac{di_{lq}}{dt} &= -\frac{R_f}{L_f} i_{lq} - \omega_{vsm} i_{ld} + \frac{v_{iq} - v_{cq}}{L_f} \\
\frac{dv_{od}}{dt} &= \omega_{vsm} v_{oq} + \frac{i_{ld} - i_{od}}{C_f} \\
\frac{dv_{oq}}{dt} &= \omega_{vsm} v_{od} + \frac{i_{lq} - i_{oq}}{C_f} \\
\frac{di_{od}}{dt} &= -\frac{R_c}{L_c} i_{od} + \omega_{vsm} i_{oq} + \frac{v_{od} - v_{bd}}{L_c} \\
\frac{di_{oq}}{dt} &= -\frac{R_c}{L_c} i_{oq} - \omega_{vsm} i_{od} + \frac{v_{oq} - v_{bq}}{L_c}
\end{aligned}\right\} \quad (1)$$

Power electronic converters control voltage and current using switches, capacitors, inductors and resistors. The modulation index which establishes how much of the dc input voltage appears at the output, controls the output voltage in an inverter. The inverter voltage is typically analyzed in the dq reference frame as v_{id} and v_{iq}. The average output voltage is given by the product of the dc voltage and the modulation indices (m_d, m_q). Neglecting PWM and switching delays, the inverter output closely follows the reference voltage $(v_{ld,ref}, v_{lq,ref})$, ensuring accurate voltage generation as mentioned in Equation 2 and Equation 3.

$$\left.\begin{aligned}
[m_d, m_q] &= \frac{[v_{ld,ref}, v_{lq,ref}]}{V_{dc}} \\
[v_{id}, v_{iq}] &\approx [m_d, m_q] V_{dc}
\end{aligned}\right\} \quad (2)$$

Therefore,

$$[v_{id}, v_{iq}] = [v_{ld,ref}, v_{lq,ref}] \quad (3)$$

2.1.2 Active and reactive power control loop

The active and reactive power loops of a VSG work together to simulate the dynamic behavior of a synchronous machine. The active power loop ($P - f$ $loop$) as shown in Fig. 2, regulates the system frequency and allows the VSG to provide inertial response and stable load sharing by altering the converter's phase angle in response to active power output through droop control, virtual inertia, and damping.

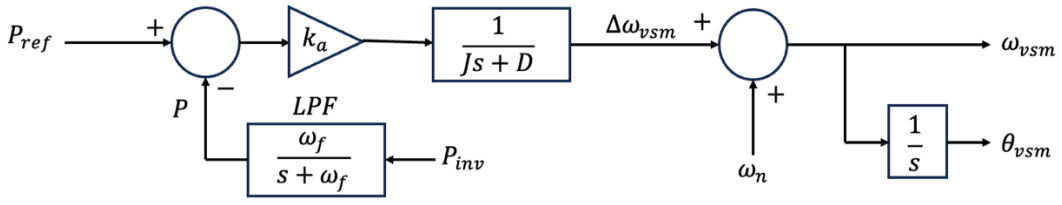

Fig. 2: Active power loop

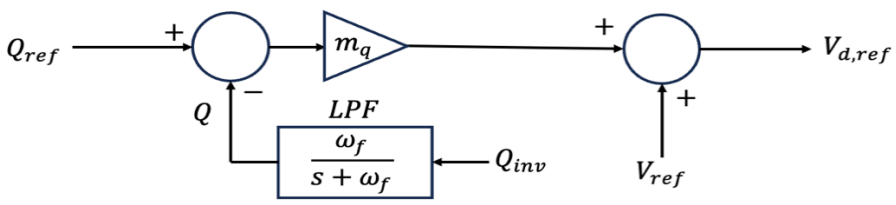

Fig. 3: Reactive power loop

Meanwhile, the reactive power loop ($Q - V\ loop$) as shown in Fig. 3, uses a voltage droop mechanism to modify the internal voltage magnitude in response to reactive power demand, maintain in response to reactive power demand, maintaining voltage stability and enabling suitable reactive power sharing. Together, these loops ensure that the VSG can control both frequency and voltage, enhancing system stability and grid-friendly operation.

The instantaneous active power and reactive power of the inverter are calculated based on Equation 4.

$$\left.\begin{aligned} p_{inv} &= \frac{3}{2} \times \left(v_{od} i_{od} + v_{oq} i_{oq}\right) \\ q_{inv} &= \frac{3}{2} \times \left(v_{oq} i_{od} + v_{od} i_{oq}\right) \end{aligned}\right\} \quad (4)$$

In order to remove high-frequency noise from the power computation, a low-pass filter is used. The filtered active and reactive power P_{inv} and Q_{inv} can be expressed in differential form as shown in Equation 5.

$$\left.\begin{aligned} \frac{dP_{inv}}{dt} &= \omega_f(-P_{inv} + p_{inv}) \\ \frac{dQ_{inv}}{dt} &= \omega_f(-Q_{inv} + q_{inv}) \end{aligned}\right\} \quad (5)$$

where, ω_f is the cut-off frequency of the low-pass filter.

Likewise, the virtual damping, droop characteristics, and virtual inertia can be incorporated in Equation 6.

$$\left.\begin{aligned} \frac{d\Delta\omega_{vsm}}{dt} &= \frac{1}{J}\left(\frac{P_{ref} - P_{inv}}{k_a} - D\Delta\omega_{vsm}\right) \\ \omega_{vsm} &= \omega_n + \Delta\omega_{vsm} \\ \frac{d\theta_{vsm}}{dt} &= \omega_{vsm} \\ v^*_{od,ref} &= v_{d,ref} + m_q\left(Q_{ref} - Q_{inv}\right) \\ v^*_{oq,ref} &= v_{q,ref} \end{aligned}\right\} \quad (6)$$

where, k_a is the droop coefficient, J is the virtual inertia, ω_n is the nominal frequency, and m_q is the reactive power droop coefficient.

The power angle of the inverter with respect to reference inverter can be written in Equation 7.

$$\frac{d\delta_{vsm}}{dt} = \omega_{vsm} - \omega_{ref} \quad (7)$$

where, ω_{vsm} and ω_{ref} are the virtual angular frequency and reference angular frequency of the inverter, respectively.

2.1.3 Virtual impedance, voltage and current controller

Virtual impedance is a key control strategy that makes an inverter behave like it makes an inverter behave like it has certain electrical impedance. It dramatically improves stability, current sharing, harmonic rejection, and grid-forming capability especially in modern converter dominated power systems.

In order to generate a control signal for the voltage controller, the virtual impedance gets the reference voltage from the reactive control loop. The voltage across the capacitor is influenced by the virtual impedance's output current. The reference voltage for the voltage controller can be generated by

Equation 8.

$$\left.\begin{aligned} v_{od,ref} &= v^{*}_{od,ref} - i_{od}R_v + i_{oq}\omega_{vsm}L_v \\ v_{oq,ref} &= v^{*}_{oq,ref} - i_{oq}R_v - i_{od}\omega_{vsm}L_v \end{aligned}\right\} \quad (8)$$

Equation 9 represents the differential equation for the voltage controller as shown in Fig. 4 adapted from (D'Arco et al., 2015; Neupane, 2025; Neupane et al., 2024). The output voltage of the voltage source inverter (VSI) is regulated using a conventional Proportional-Integral (PI) controller.

$$\left.\begin{aligned} i_{ld,ref} &= K_{pv}\left(v_{od,ref} - v_{od}\right) + K_{iv}\gamma_d + i_{odi} - \omega_{vsm}C_f v_{oq} \\ i_{lq,ref} &= K_{pv}\left(v_{oq,ref} - v_{oq}\right) + K_{iv}\gamma_q + i_{oqi} - \omega_{vsm}C_f v_{od} \\ \frac{d\gamma_d}{dt} &= v_{od,ref} - v_{od} \\ \frac{d\gamma_q}{dt} &= v_{oq,ref} - v_{oq} \end{aligned}\right\} \quad (9)$$

where, K_{pv} and K_{iv} are the proportional and integral control gains of the voltage controller loop.

Equation 10 represents the differential equation for the current controller as shown in Fig. 4 adapted from (D'Arco et al., 2015; Neupane, 2025; Neupane et al., 2024). The output current of the VSI is regulated using a conventional PI controller.

$$\left.\begin{aligned} v_{ld,ref} &= K_{pc}\left(i_{ld,ref} - i_{ld}\right) + K_{ic}\zeta_d + v_{odi} - \omega_{vsm}L_f i_{lq} \\ v_{lq,ref} &= K_{pc}\left(i_{lq,ref} - i_{lq}\right) + K_{ic}\zeta_q + v_{oqi} - \omega_{vsm}L_f i_{ld} \\ \frac{d\zeta_d}{dt} &= i_{ld,ref} - i_{ld} \\ \frac{d\gamma_q}{dt} &= i_{lq,ref} - i_{lq} \end{aligned}\right\} \quad (10)$$

where, K_{pc} and K_{ic} are the proportional and integral control gains of the current controller loop.

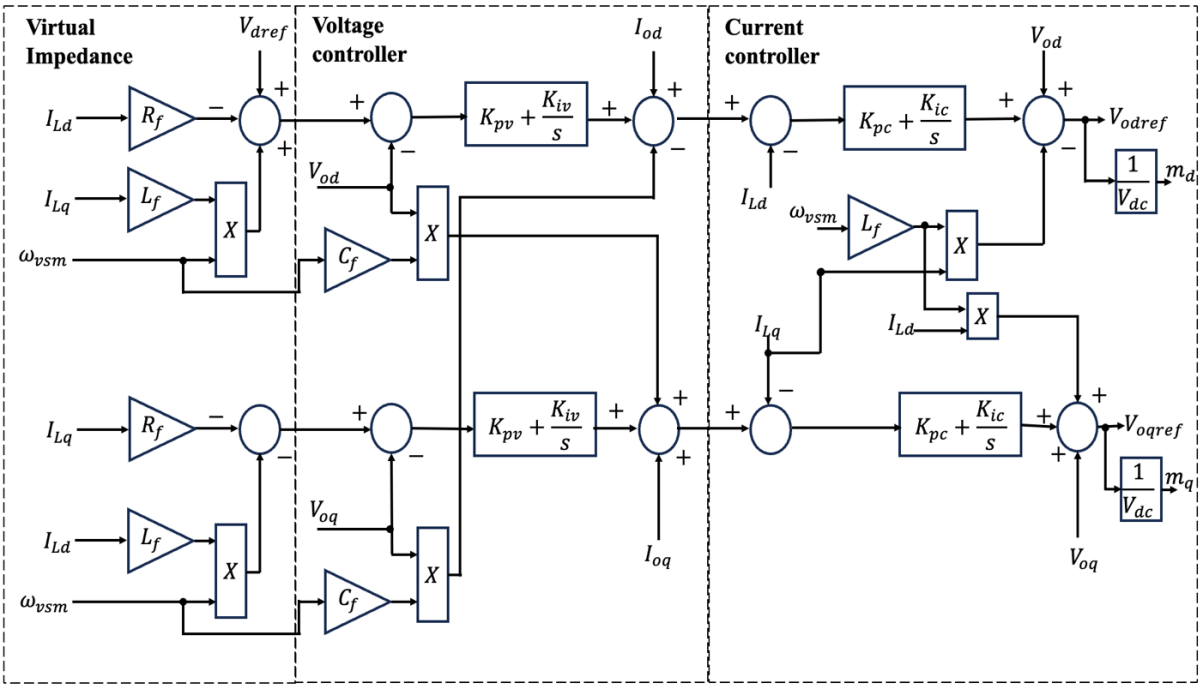

Fig. 4: Virtual impedance, voltage controller, and current controller loop for inverter.

3. Simulation model

The MATLAB/Simulink model of a grid-connected inverter using virtual synchronous machine (VSM) based on virtual inertia control, shown in Fig. 5, mics the behavior of a synchronous generator by providing virtual inertia and regulating the active and reactive power.

The upper part of the model represents the physical power stage, where a DC/AC inverter supplies filter connected to the grid. The measured voltages and currents are transformed from abc to

dq coordinates using the virtual angle generated by the VSM. Active power and reactive power are calculated in dq frame and used in the VSM control loop, where active power errors regulate the voltage through droop control. this structure eliminates the need for a PLL and enables synchronous machine-like behavior. The inner voltage and current loops track the VSM commands and generate PWM signals for the inverter.

The simulations are caried out in MATLAB/Simulink (R2024a) with a sampling time $T_s = 5\mu s$ of for a total duration of 1 second on a MacBook Air M1 (8 GB RAM).

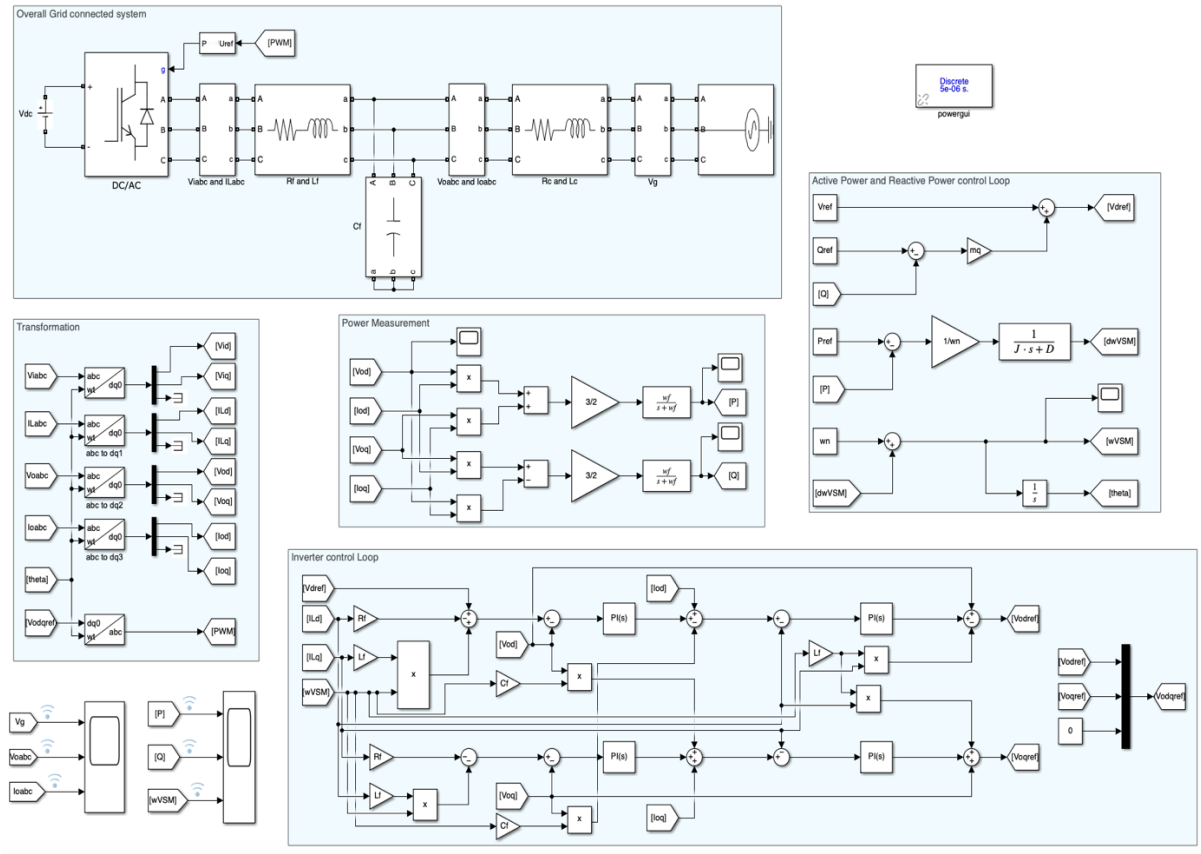

Fig. 5: Overall Simulink model of grid connected VSG.

3.1 Data Parameters for simulation

The crucial step of defining the operational parameters for the simulation is summarized comprehensively in Table 1. This table details every constant required to model the Grid-Connected Virtual Synchronous Machine (VSM) system, ranging from physical hardware specifications to the inner controller gains (Neupane, 2025).

Table 1: Parameters used for detailed simulation and data generation.

Parameters	Values	Parameters	Values
Converter DC voltage $(\boldsymbol{V_{dc}})$	$1000\ V$	Grid coupling inductance (L_c)	$0.15\ mH$
Grid voltage $(\boldsymbol{V_g})$	$400\ V$	Reference active power (P_{ref})	$50\ kW$
$(\boldsymbol{V_{dref}})$	$\sqrt{\frac{2}{3}} \times 400\ V$	Reference reactive power (Q_{ref})	$0\ Var$
$(\boldsymbol{V_{qref}})$	$0\ V$	Active power droop coefficient (k_a)	3.14×10^{-3}

System nominal frequency $(\boldsymbol{f})$	$50\ Hz$	Reactive power droop coefficient (m_q)	1×10^{-5}
Filter cut-off frequency $(\boldsymbol{\omega_f})$	4π	Voltage controller Proportional gain (K_{pv})	3
PWM switching frequency $(\boldsymbol{f_c})$	$10\ kHz$	Voltage controller Integral gain (K_{iv})	400
Filter resistance $(\boldsymbol{R_f})$	$0.07\ \Omega$	Current controller Proportional gain (K_{pc})	5
Filter inductance $(\boldsymbol{L_f})$	$5.2\ mH$	Current controller Integral gain (K_{ic})	10
Filter capacitance $(\boldsymbol{C_f})$	$100\ \mu F$	Virtual inertia constant (J)	$0.05\ s$
Grid coupling resistance $(\boldsymbol{R_c})$	$0.05\ \Omega$	Virtual damping constant (D)	10

4. Results

This section presents the dynamic response of the VSM for different virtual inertia (J) and damping (D) values. Since inertia strongly influences transient behavior, varying J allows the VSM to emulate different to emulate different levels of oscillations and energy storage. The response of active power (P) and reactive power (Q) and angular velocity (ω_{vsm}) are evaluated for different values of $J = 0.01, 0.025, 0.05$ and 0.075 under step changes in power reference. In addition, the effect of damping was studied $D = 10, 40, 70$ and 100 to assess its role in oscillation suppression, settling time, and system stability.

4.1 Response for different values of inertia (J) keeping damping (D) constant

The system's transient response of active power (P) in Fig. 6, reactive power (Q) in Fig. 7 and angular velocity (ω_{vsm}) in Fig. 8 following over a 1 second period for four different values of J keeping $D = 10$ constant, were recorded.

4.1.1 Active power (P) of inverter

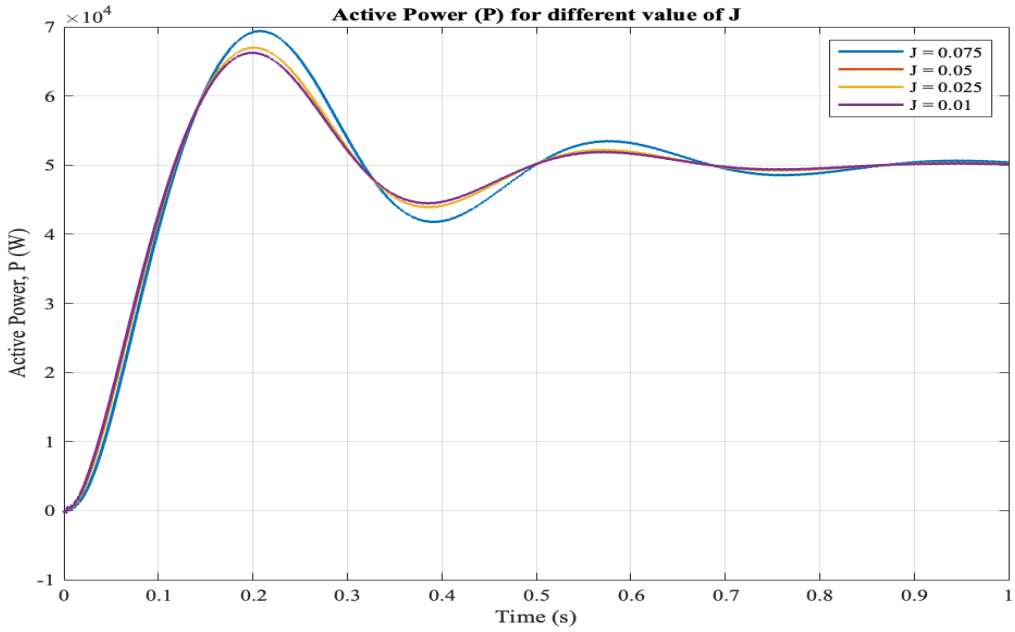

Fig. 6: Active power responses for different value of J.

Fig. 6 reveals the active power (P) response of the inverter at various levels of virtual inertia (J), keeping the damping constant at D= 10. Reference active power is 50kW.The transient response of the system changes a lot with the inertia value. With J=0.075, the active power first goes up to a peak of about 69kW around 0.2s, which is an overshoot of almost 38% against the reference power. Besides, the response also has bigger oscillations and a longer time is needed for it to get back to 50kW steady-state. When the inertia value becomes smaller, the overshoot and the oscillatory behavior will be less. With J=0.01, the peak active power goes down to about 66kW, meaning an overshoot of around 32%. Besides, the oscillations are smaller and the response gets back to normal faster than with higher inertia. Ultimately, the active power in all the cases reacts to the reference value of 50kW after the transient oscillations. The findings show that by raising the virtual inertia, the inertial support is enhanced. Then again, the oscillation amplitude and the settling time are also increased in the grid-connected VSG system.

4.1.2 Reactive power (Q) of inverter

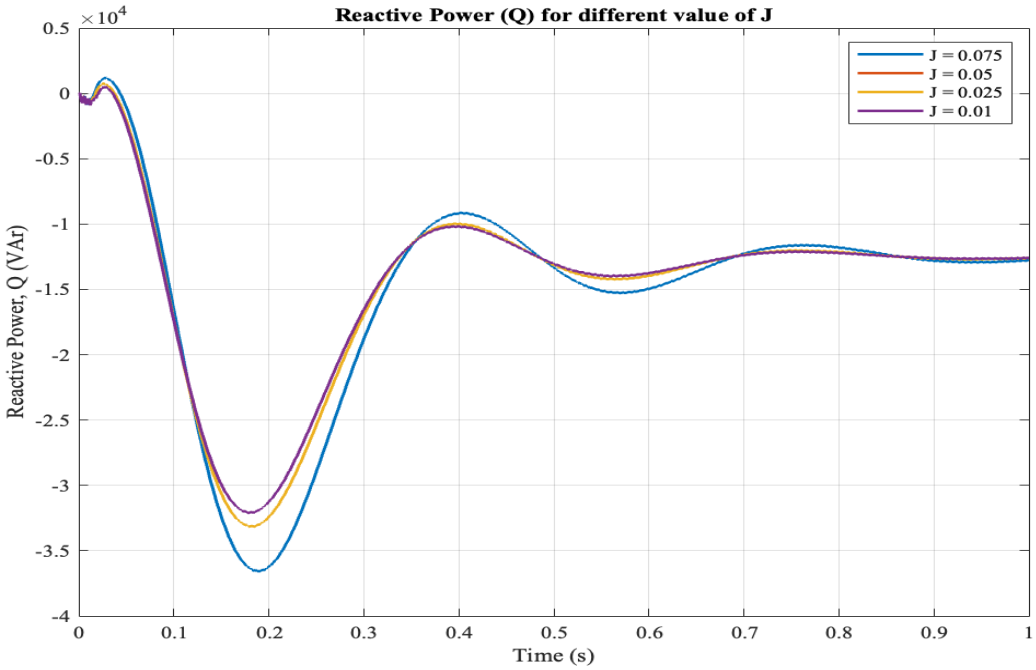

Fig. 7: Reactive power responses for different value of *J*.

Fig. 7 presents the inverter reactive power outputs with the four different virtual inertia constants (J = 0.01, 0.025, 0.05, and 0.075 kg·m²) simulated over 1 second period. All four scenarios initially feature a small positive overshoot of about 1 kVAr, then they fall sharply into a negative region, where the greatest differences are manifested during the first negative peak (time t approx. 0.18-0.20 sec.). At this point, J = 0.075 causes the largest undershoot of roughly −37 kVAr against −31 kVAr for J = 0.01, which is a 19.4% rise in the peak reactive power deviation confirming that more virtual inertia increases the magnitude of transient excursions. The subsequent curves represent responses that are damped oscillations, while the difference between the curves keeps on reducing, which is an indication that the system is naturally damping the inertia-induced differences over time. After time 0.70 second, the four responses settle down to the same value of about −12.5 kVAr, which is consistent within reality the J value only changes the transient dynamics and not the steady-state operating condition.

The results highlight an important inertia-oscillation trade-off, as increasing the J values leads to more inertial support, but also results in bigger reactive power swings and a slightly longer settling time of approximately 0.75s compared to 0.65s for the smallest inertia case.

4.1.3 Angular velocity (ω_{vsm}) of inverter

Fig. 8 shows the angular velocity (ω_{vsm}) of the virtual synchronous machine during 1 second simulation for J = 0.01, 0.025, 0.05, and 0.075 kg·m². At first, the four cases (ω_{vsm}) peak the same, at about 330 rad/s within the first 0.02 s. After that, the angular velocity falls steeply to the first negative minimum at about t ≈ 0.20–0.22 s. At this minimum, J = 0.075 gives the lowest point of about 308 rad/s, whereas the cases with lower inertia (J = 0.01 and 0.025) settle a bit higher, at about 309.5 rad/s, a very slight but regular difference of ~1.5 rad/s, which shows that bigger virtual inertia leads to bigger frequency undershoot since the inertial dynamics' response are slower. After the minimum, the angular velocity rises to the second maximum of about 316-317 rad/s at t ≈ 0.38-0.40 s. Again J = 0.075 shows the slightly bigger overshoot, but ultimately, the curves cross the small second trough at t ≈ 0.55 s, about 313.5 rad/s. After t ≈ 0.70 s, all responses reach a stable operating level of angular velocity of about 314 rad/s (which corresponds to the normal frequency of the grid of 50 Hz, i.e. 2π × 50 ≈ 314.16 rad/s), and the cases with higher J take a bit longer to completely stabilize. The findings here show that the virtual inertia constant J determines the oscillatory transient pattern of the inverter's angular velocity but does not affect the final steady-state frequency, which is in line with the same inertia-oscillation compromise noticed in the reactive power response.

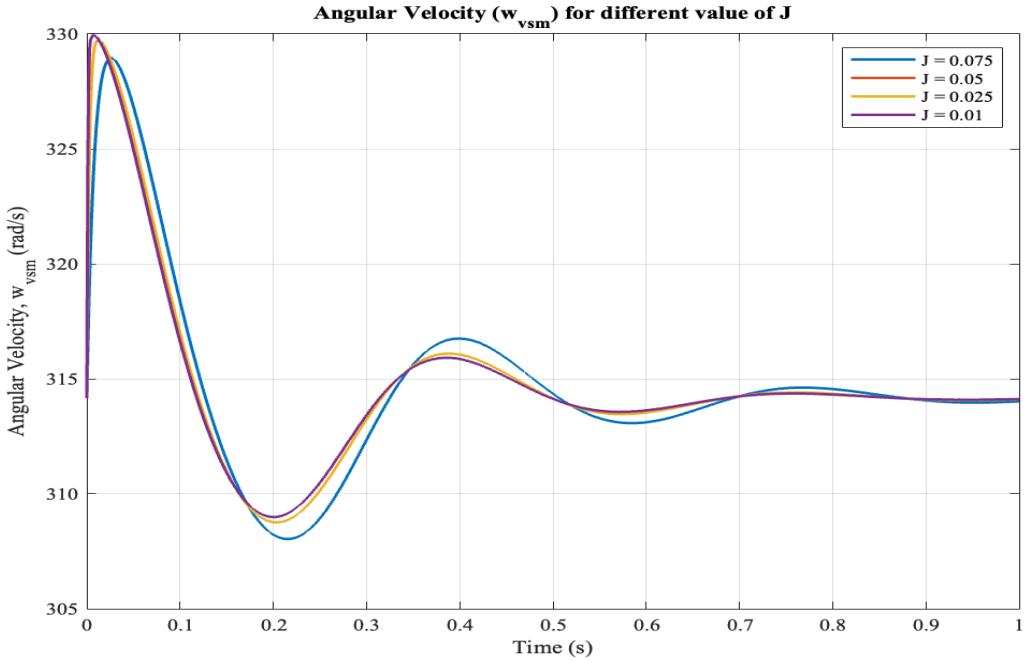

Fig. 8: Angular velocity responses for different value of J.

4.2 Response for different values of damping (D) keeping inertia (J) constant

The system's transient response of active power (P) in Fig. 9, reactive power (Q) in Fig. 10 and angular velocity (ω_{vsm}) in Fig. 11 following over a 1 second period for four different values of D keeping $J = 0.05$ constant, were recorded.

4.2.1 Active power (P) of inverter

Fig. 9 shows the inverter's active power transient response for four damping coefficient values (D = 10 40 70, and 100) while the virtual inertia constant is fixed at J = 0.05 kg·m². The outcomes show that the transient behavior depends strongly and monotonically on D, with lower damping values giving rise to the quickest but also most oscillatory responses. For D = 10, the active power increase is sharp, and it peaks at about 67,000 W at t ≈ 0.20 s after which it drops and stabilizes, this corresponds to an overshoot of approximately 34% above the steady-state value. Then again, D = 40 results in a lower peak of around 52,000 W near t ≈ 0.50 s, whereas D = 70 and D = 100 give overdamped, monotonically increasing

responses that reach the steady state without any overshoot, approximately 48,000–50,000 W at t ≈ 0.90–1.0 s. The four scenarios come to the same steady-state active power of about 50,000 W (50 kW), showing that the damping coefficient D only influences the dynamic patterns of the response and not the final operating point. This implies a basic damping response speed trade-off: lower D values speed up the power delivery initially but lead to significant overshoot and oscillation Though higher D values reduce the transient variations but at the expense of a Much slower rise time, with D = 100 taking almost the entire 1-second duration to reach steady state versus D = 10 which settles in about 0.60 s.

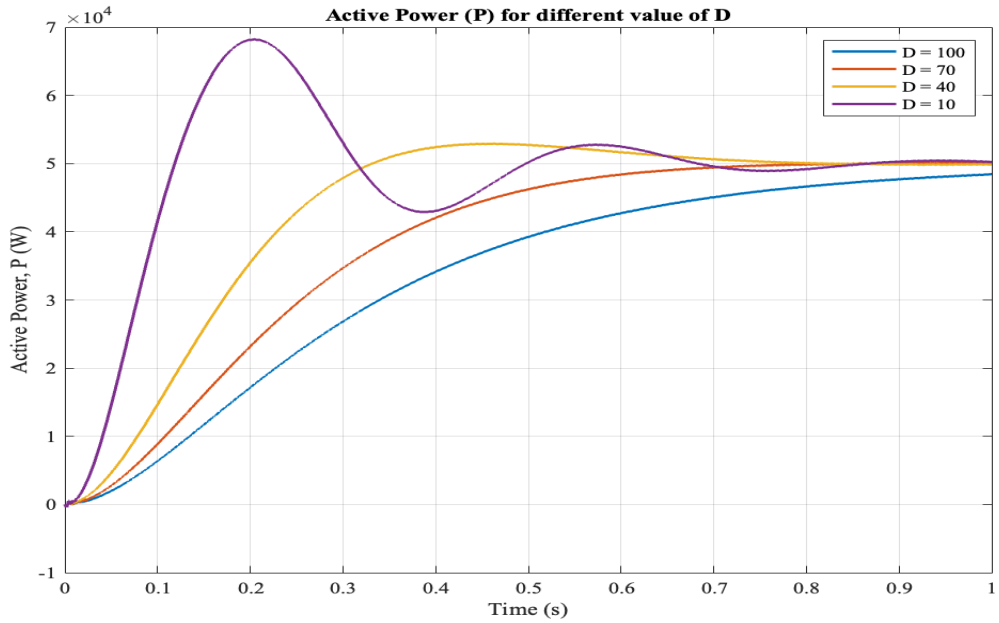

Fig. 9: Active power responses for different value of D.

4.2.2 Reactive power (Q) of inverter

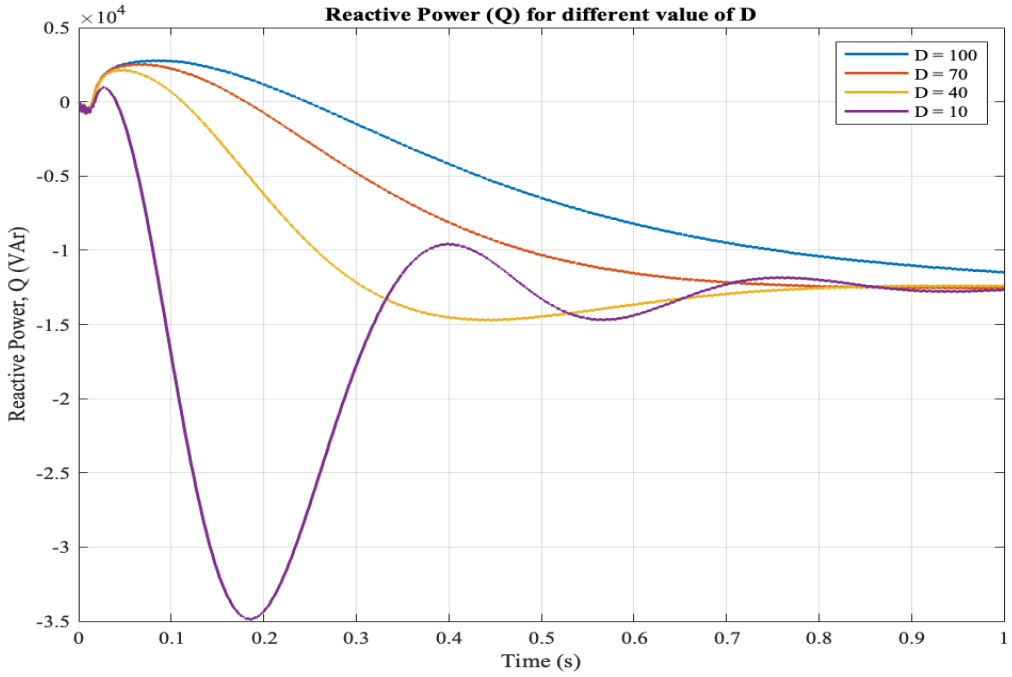

Fig. 10: Reactive power responses for different value of D.

The Fig. 10 displays the transient response of reactive power for different damping values (D = 10 40 70 and 100)

at a constant moment of inertia of J = 0. 05 kg·m². The 4 scenarios record a small positive peak, nearly +2 kVAr, for the first 0. 05 s after which they poorly. The response that is more dramatic is that of D=10, which dips to a deep negative valley of about −33 kVAr at t ≈ 0. 18 s, before getting better, it also shows clear underdamped oscillatory behavior with a secondary peak near −10000 VAr at t ≈ 0. 40 s. Then again, D=40 displays slower and more steady decline, going down to a moderately low level roughly -13000 VAr at t ≈ 0.35 s with only slight oscillations, whereas D=70 and D=100 are two overdamped systems which, without a single point of bouncing back or undershooting, gradually moving downward and hitting -1 to -11 kVAr at t ≈ 0. 50-0. 60 s. The very different behavior of D=10 and D=100 for maximum reactive power deviation i.e., around 33 kVAr vs a smooth transition, demonstrates the importance of the damping coefficient in minimizing reactive power excursions. All the 4 plots reach the steady-state value at -12.5 kVAr after each having their peak at different times, a clear indication that the damping factor D has an influence on the transient response but not on the final steady-state value. More damping results in less reactive power oscillations and less peak deviations albeit with a tradeoff of slower initial transient response as indicated by the results.

4.1.3 Angular velocity (ω_{vsm}) of inverter

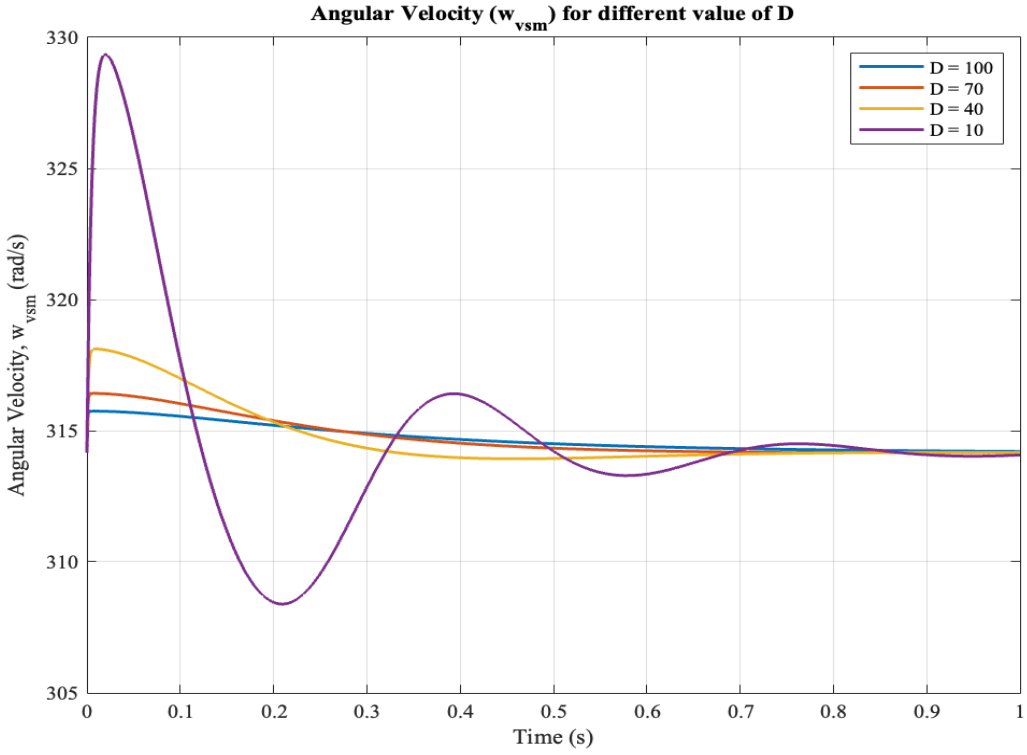

Fig. 11: Angular velocity responses for different value of D.

Fig. 11 shows the response of the angular velocity of the virtual synchronous machine for various damping coefficients (D = 10 40 70, and 100) and a moment of inertia J = 0.05 kg·m² fixed. While in the previous examples all the curves showed the same initial peak, the responses here already differ at t = 0, highlighting the great impact of oscillation damping on the frequency deviation rate. For D = 10, the overshoot reaches about 329 rad/s at a very short time of 0.02 s. The other cases with D = 40, 70, and 100 have lower overshoot values that are approximately 318, 317, and 316 rad/s respectively, which shows how higher damping coupled with the initial frequency deviation is limited to the lowest damping case by almost 13 rad/s. D = 10 not only peaks first but also dips the deepest to about 308.5 rad/s around 0.20 seconds before it starts to recover through a secondary oscillation near 316 rad/s at about 0.40 seconds. A peak-to-trough swing of total approximately 20.5 rad/s clearly characterizes the underdamped response. But, D = 40 gently goes down to a patchy trough of nearly 314 rad/s at about 0.30 seconds with only a tiny oscillation and the wave crests of D = 70 and D = 100 slowly and monotonically approach the steady state after the trough without dip, this way confirming the overdamping nature of these two cases. After that, starting from approximately 0.70 seconds, all four graphs tend to the nominal steady-state angular velocity of about 314 rad/s (which corresponds to 50 Hz) again. Yet, D = 10 still shows the longest

time to settle completely due to its continually low-amplitude oscillations. The study leading to these results reveals In reality the damping coefficient D has an overriding influence in the regulation of frequency deviation amplitude as well as the degree of oscillation suppression, whereby greater values of D can enforce better frequency stability although it could mean a slower initial dynamic response.

5. Discussion

In this paper, different and yet complementary functions of the virtual inertia constant (J) and the damping coefficient (D) in governing the transient behavior of a grid-forming Virtual Synchronous Machine (VSM) are analytically revealed first. Through a control-theoretic lens, the VSM swing equation is a second-order nonlinear dynamical system, in which J mainly modulates the natural frequency of the system, while D directly impacts the damping ratio. This way the mutual tuning of these two variables effectively controls the stability margins, the transient energy exchange, and the convergence speed of the inverter-based resource.

Simulation outputs demonstrate that an increase in J leads to a decrease not only in the effective damping ratio but also in the system's natural frequency, which comes out as a slower system behavior with enhanced oscillatory modes in angular velocity, active power, and reactive power. Higher inertia, on one hand, basically enhances frequency ride-through capability by restraining rapid rate-of-change-of-frequency (RoCoF). But it excites the electromechanical-like oscillations that are hardly damped and So prolongs the time it takes to reach stability. In contrast, lower inertia levels correspond to the system's poles relocating further left in the complex plane, which means that the transient response is quicker and the oscillation amplitude is smaller. These results are in line with the latest grid-forming inverter work that reveals that too much virtual inertia can reduce small-signal stability and lead to more intensity of power oscillations in low-inertia grids. The damping coefficient D serves as the major stabilizing factor by a direct way in that it increases the damping ratio of the swing dynamics. Damping at a low level produces under-damped system behavior with a significant overshoot and oscillations that do not die out, indicating that there is not enough dissipation of transient energy. Then again, very high damping leads to an overdamped type of response where the suppression of oscillations goes together with slower synchronization and a drop in the dynamic activeness. Moderate damping values (D = 40 to 70) come close to a critical damping level leading to, in fact, the best balancing between a rapidly changing transient scenario and the control of oscillations. Such a reaction is very much in line with the highly control-oriented grid-forming literature, whereby virtual damping is regarded as a prerequisite for a large frequency stability and power regulation scope.

Overall, the results highlight a fundamental design trade-off inherent to grid-forming VSM control: the inertia constant governs the magnitude and rate of the inertial frequency response, while the damping coefficient regulates the dissipation of transient energy and stabilization speed. Optimal VSM performance is achieved by selecting a moderately low inertia to limit oscillatory energy injection and carefully tuning damping to ensure rapid, well-damped convergence. This tuning philosophy supports emerging consensus in grid-forming inverter research, emphasizing that stability-oriented damping design is more critical than simply increasing virtual inertia in future low-inertia power systems.

6. Conclusion

This work assessed the transient stability and dynamic behavior of a grid-connected Virtual Synchronous Generator (VSG) with virtual impedance control, focusing on the impacts of the virtual inertia constant (J) and damping coefficient (D) In particular during the power reference step changes. It is concluded that J controls mainly the response time and the ability to withstand rapid disturbances. Increasing the inertia proportionally decreases the effective damping, which in turn results in larger and more persistent oscillations of the active power, reactive power, and angular velocity. However, lower

inertia leads to quicker recovery but also increases the vulnerability to initial transients. Having a middle range inertia value (J = 0.05) is a good trade-off between the benefits of inertia and the settling time. But it was found that the damping coefficient makes a difference in suppressing the oscillations. Inadequate damping leads to unstable and underdamped oscillations, whereas excessive damping results in slow and overdamped motions. The mix of damping values in the range $(D = 40 \text{ to } 70)$ gives the optimum dynamic performance, with a combination of rapid settling and minimum overshoot. The findings establish the importance of the combined tuning of inertia and damping to produce a quick, well-damped response for VSM. Coupled with the right selection of parameters, the VSM is capable of being a dependable grid-support means that makes easier renewable integration and at the same time, does not compromise system stability and power quality.

7. Recommendation for Future Work

Further research to deepen this study could explore the joint optimization of virtual inertia J and damping D beyond fixed parameter tuning. Finding the best pair of these two parameters is a must to achieve a more effective damping and a smaller transient overshoot. At the same time, adaptive and data-driven control methods could be taken into account, which adjust J on the fly based on the extent of the grid disturbance, Because of this combining rapid response and strong stability. What is more, the VSM controller should be tested in weak grid scenarios, and new decoupling techniques for the inner current loop need to be engineered to mitigate the power active–reactive coupling during transients.

Acknowledgements

The team of authors would like to thank Associate Professor Bhrigu Bhattarai, Assistant Professors Sandeep Dhami, Suraj Shrestha, Menaka Karki, Nawaraj Poudel, Deependra Neupane, and the Department of Electrical Engineering at Institute of Engineering, Pashchimanchal Campus Pokhara Nepal for their insightful feedback, excellent suggestions, and collaborative spirit.

References

Bevrani, H., Ise, T., & Miura, Y. (2014). Virtual synchronous generators: A survey and new perspectives. *International Journal of Electrical Power & Energy Systems*, *54*, 244–254. https://doi.org/10.1016/j.ijepes.2013.07.009

Citro, C., Al-Numay, M., Siano, P., & Alhelou, H. H. (2024). Experimental evaluation of virtual synchronous generators with high regulation performance to enhance AC–DC grid interconnections. *International Journal of Electrical Power and Energy Systems*, *158*, 109964. https://doi.org/10.1016/j.ijepes.2024.109964

D'Arco, S., & Suul, J. A. (2013). Virtual synchronous machines—Classification of implementations and analysis of equivalence to droop controllers for microgrids. *2013 IEEE Grenoble Conference*, 1–7. https://doi.org/10.1109/PTC.2013.6652456

D'Arco, S., Suul, J. A., & Fosso, O. B. (2015). Small-signal modeling and parametric sensitivity of a virtual synchronous machine in islanded operation. *International Journal of Electrical Power & Energy Systems*, *72*, 3–15. https://doi.org/10.1016/j.ijepes.2015.02.005

Deng, J., Xia, N., Yin, J., Jin, J., Peng, S., & Wang, T. (2020). Small-Signal Modeling and Parameter Optimization Design for Photovoltaic Virtual Synchronous Generator. *Energies*, *13*(2), 398. https://doi.org/10.3390/en13020398

Ding, X., Lan, T., & Dong, H. (2019). Control Strategy and Stability Analysis of Virtual Synchronous Generators Combined with Photovoltaic Dynamic Characteristics. *JOURNAL OF POWER ELECTRONICS*, *19*(5), 1270–1277.

He, P., Li, Z., Jin, H., Zhao, C., Fan, J., & Wu, X. (2023). An adaptive VSG control strategy of battery energy storage system for power system frequency stability enhancement. *International Journal of Electrical Power & Energy Systems*, *149*, 109039. https://doi.org/10.1016/j.ijepes.2023.109039

Jakhar, S., Soni, M. S., & Gakkhar, N. (2016). Historical and recent development of concentrating photovoltaic cooling technologies. *Renewable and Sustainable Energy Reviews*, *60*, 41–59. https://doi.org/10.1016/j.rser.2016.01.083

Li, C., Yang, Y., Mao, X., Xiong, X., & Dragicevic, T. (2025). Modeling, control and stabilization of virtual synchronous generator in future power electronics-dominated power systems: A survey of challenges, advances, and future trends. *International Journal of Electrical Power & Energy Systems*, *171*, 111001. https://doi.org/10.1016/j.ijepes.2025.111001

Liang, W., Liu, Y., & Shen, Y. (2023). Active Power Control Integrated With Reactive Power Compensation of Battery Energy Stored Quasi-Z Source Inverter PV Power System Operating in VSG Mode. *IEEE Journal of Emerging and Selected Topics in Power Electronics*, *11*(1), 339–350. https://doi.org/10.1109/JESTPE.2021.3137397

Liu, Y., Hao, M., He, Y., Zang, C., & Zeng, P. (2019). Review and Applications of Virtual Synchronous Machines Technologies. *2019 IEEE Innovative Smart Grid Technologies - Asia (ISGT Asia)*, 593–598. https://doi.org/10.1109/ISGT-Asia.2019.8881466

Moore, P., Alimi, O. A., & Abu-Siada, A. (2025). A Review of System Strength and Inertia in Renewable-Energy-Dominated Grids: Challenges, Sustainability, and Solutions. *Challenges*, *16*(1), 12. https://doi.org/10.3390/challe16010012

Neupane, D. (2025). Data-driven modelling of grid-connected virtual synchronous machine dynamics using optimized dynamic mode decomposition and SINDy. *Applied Mathematics in Science and Engineering*, *33*(1), 2576864. https://doi.org/10.1080/27690911.2025.2576864

Neupane, D., & Poudel, N. (2024). Small-Signal Stability Modeling, Sensitivity Analysis, and Parameter Optimization of Improved Virtual Synchronous Machine Based Standalone Inverter. *Electric Power Components and Systems*, *52*(7), 1022–1038. https://doi.org/10.1080/15325008.2023.2238205

Neupane, D., Poudel, N., Neupane, D., & Poudel, N. (2024). Small-Signal Stability Analysis of Virtual Impedance Based Parallel Inverters. In *Bridging Eigenvalue Theory and Practice—Applications in Modern Engineering*. IntechOpen. https://doi.org/10.5772/intechopen.1006731

Paquette, A. D., & Divan, D. M. (2015). Virtual Impedance Current Limiting for Inverters in Microgrids With Synchronous Generators. *IEEE Transactions on Industry Applications*, *51*(2), 1630–1638. https://doi.org/10.1109/TIA.2014.2345877

Qu, S., & Wang, Z. (2021). Cooperative Control Strategy of Virtual Synchronous Generator Based on Optimal Damping Ratio. *IEEE Access*, *9*, 709–719. https://doi.org/10.1109/ACCESS.2020.3046626

Rajak, M. K., & Pudur, R. (2025). Multiobjective adaptive predictive virtual synchronous generator control strategy for grid stability and renewable integration. *Scientific Reports*, *15*(1), 9241. https://doi.org/10.1038/s41598-025-93721-y

Rocabert, J., Luna, A., Blaabjerg, F., & Rodríguez, P. (2012). Control of Power Converters in AC Microgrids. *IEEE Transactions on Power Electronics*, *27*(11), 4734–4749. https://doi.org/10.1109/TPEL.2012.2199334

Sangwongwanich, A., Yang, Y., Blaabjerg, F., & Sera, D. (2017). Delta Power Control Strategy for Multistring Grid-Connected PV Inverters. *IEEE Transactions on Industry Applications*, *53*(4), 3862–3870. https://doi.org/10.1109/TIA.2017.2681044

Tahir, W., Farhan, M., Bhatti, A. R., Butt, A. D., & Farid, G. (2024). A modified control strategy for seamless switching of virtual synchronous generator-based inverter using frequency, phase, and voltage regulation. *International Journal of Electrical Power & Energy Systems*, *157*, 109805. https://doi.org/10.1016/j.ijepes.2024.109805

Worthmann, K., Kellett, C. M., Braun, P., Grüne, L., & Weller, S. R. (2015). Distributed and Decentralized Control of Residential Energy Systems Incorporating Battery Storage. *IEEE Transactions on Smart Grid*, *6*(4), 1914–1923. https://doi.org/10.1109/TSG.2015.2392081

Yan, G., Zhang, X., Zhang, S., & Yang, H. (2018). A Novel Virtual Inertial Control Strategy for Double-Stage PV Generation. *2018 2nd IEEE Conference on Energy Internet and Energy System Integration (EI2)*, 1–5. https://doi.org/10.1109/EI2.2018.8581891

Yao, G., Lu, Z., Benbouzid, M., Tang, T., & Han, J. (2015). A virtual synchronous generator based inverter control method for distributed generation systems. *IECON 2015 - 41st Annual Conference of the IEEE Industrial Electronics Society*, 002112–002117. https://doi.org/10.1109/IECON.2015.7392413

Zarina, P. P., Mishra, S., & Sekhar, P. C. (2014). Exploring frequency control capability of a PV system in a hybrid PV-rotating machine-without storage system. *International Journal of Electrical Power & Energy Systems*, *60*, 258–267. https://doi.org/10.1016/j.ijepes.2014.02.033

Appendix: Model availability

The MATLAB/Simulink created for this study will be available in GitHub link: https://github.com/075bel032/Grid-connected-VSM-based-on-Virtual-inertia-control.git